Remote Sensing of Environment 134 (2013) 342–354

Contents lists available at SciVerse ScienceDirect

Remote Sensing of Environment

journal homepage: www.elsevier.com/locate/rse

Using Hyperion imagery to monitor the spatial and temporal distribution of colored dissolved organic matter in estuarine and coastal regions

Weining Zhu [a], Yong Q. Tian [a,*], Qian Yu [b], Brian L. Becker [a]

[a] Institute for Great Lakes Research, Department of Geography, Central Michigan University, United States
[b] Department of Geosciences, University of Massachusetts, Amherst, United States

ARTICLE INFO

Article history:
Received 30 November 2012
Received in revised form 13 March 2013
Accepted 14 March 2013
Available online xxxx

Keywords:
CDOM
Hyperspectral remote sensing
Estuaries
EO-1 hyperion
QAA-CDOM
Climate impacts
Land-surface processes

ABSTRACT

Establishing a link between the optical and biogeochemical properties of near-shore waters continues to be a challenge for both riverine and estuarine areas worldwide due to terrestrial influences. This study aimed to evaluate the effectiveness of an inversion algorithm for the extraction of riverine and estuarine CDOM properties at global scales. Our CDOM evaluation focused on five aspects: 1) the range of worldwide CDOM levels, 2) spatial distribution patterns, (3) climatic influences, (4) influences of land cover change, and (5) seasonal effects. The study locations consisted of the estuarine and coastal regions of 10 major rivers spread across five continents. Our approach was to examine the QAA-CDOM algorithm by extracting CDOM properties from hundreds of EO-1 Hyperion images acquired during the last decade (2001–2011). Preliminary results showed that CDOM absorption coefficients at 440 nm within the 10 selected rivers exhibited a broad range (0.02–7.2 m^{-1}). Spatial CDOM distribution patterns showed many plumes dispersing from source areas (e.g. adjacent terrestrial vegetated areas) along the direction of flow. Seasonal variations in CDOM levels are also evident (i.e. 0.5–4.0 m^{-1}) as illustrated by the January, April, August and October images of the Volga River. CDOM levels also appeared to trend upward with the increase in forest coverage (i.e. terrestrial influence) within the watersheds studied over the last decade. Our results strongly suggest that the algorithm is effective in distinguishing riverine and estuarine CDOM levels affected by factors such as global biogeography, climate conditions and regional land surface processes.

1. Introduction

Colored dissolved organic matter (CDOM) is often used as an effective tracer for evaluating relative levels and the spatial distribution of dissolved organic carbon (DOC) in aquatic environments. CDOM is the photoactive portion of dissolved organic matter (DOM) (Ferrari et al., 1996; Mannino et al., 2008; Vodacek et al., 1997). CDOM $a_g(440)$, (absorption coefficient at 440 nm) is detectable from above the water surface remotely (i.e. in-situ, airborne or space-borne), since its chromophore property displays absorbance of light decreasing quasi-exponentially with increasing wavelength across the entire UV and visible spectrum (Kutser et al., 2005). Therefore, the quantification of relative CDOM levels via remote sensing technologies could be a valuable tool for studying ecological/environmental changes as well as carbon cycling at global scales (Tranvik et al., 2009). Remote estimation of CDOM is also relevant to aquatic ecological/limnological research in that it is a significant factor in overall light penetration, which is a critical factor of chlorophyll photosynthesis carried out by phytoplankton and other aquatic vegetation (Kirk, 1994).

Remote sensing of CDOM has been well studied in Case 1, open sea environments where CDOM concentrations are generally in low concentration and spatially homogeneous (Yu et al., 2010). CDOM in these waters is mainly autochthonous, formed from exudates and partial decomposition products of phytoplankton (Nelson & Siegel, 2001). Contrarily, relative CDOM levels in coastal waters (e.g. Case 2 waters) are usually much higher than that in open-sea environments because of influences from terrestrial biological and geochemical sources (i.e. allochthonous). The humic and fulvic acid released from the decay of detritus represents the most significant component of terrestrial/soil CDOM in riverine and near-shore environments (Coble, 1996; De Souza Sierra et al., 1994). Geochemical source means the amount of DOC in deep soils deposited thousands years ago and moved to rivers through weathering processes (Petsch et al., 2003). In addition, both chlorophyll concentrations and turbidity are typically much higher in riverine systems, when compared to open sea environments. The algorithms developed for case 1 waters may not be accurate for riverine and estuarine environments because of potential interference from solutes and suspended matter found in such waters that are not typically found in open oceans.

A remote sensing algorithm for extracting CDOM for estuarine and coastal regions (QAA-CDOM) recently was developed by Zhu and Yu (2013) and Zhu et al. (2011). The key innovation of the algorithm is

* Corresponding author. Tel.: +11 8579987898.
E-mail address: yong.tian@cmich.edu (Y.Q. Tian).

0034-4257/$ – see front matter © 2013 Elsevier Inc. All rights reserved.
http://dx.doi.org/10.1016/j.rse.2013.03.009

the capability of estimating CDOM and sediment absorption coefficients separately instead of a single combined parameter. Although the algorithm was based on both field and synthetic data worldwide, it has only been validated across 12 riverine, estuarine, and coastal sites that exhibit a limited range of climatic and geographic variation (Zhu, 2011; Yu et al., 2010; Zhu and Yu, 2013; Zhu et al., 2011). The relatively limited geographic and climatic areas to which the algorithm was applied may indeed limit its reliability across global scales that typically exhibit a much wider range of CDOM levels It is also known that temperature and precipitation are highly correlated to both riverine DOC and relative CDOM levels due to the influence of terrestrial gross primary production (GPP) and metabolic processes within the surrounding watershed (Huang & Chen, 2009; Raymond & Bauer, 2001; Tian et al., 2013). Land surface characteristics, such as vegetation types, soil carbon sinks, and hydrologic characteristics (e.g. surface runoff rates, groundwater discharge) determine CDOM sources and transport processes (Coble, 1996; De Souza Sierra et al., 1994; Tian et al., 2013). Therefore, in order to confirm the suitability of QAA-CDOM at global scales, it is necessary to examine its applicability across more varied scenarios.

Accordingly, this study aims to evaluate the feasibility of applying the QAA-CDOM model to rivers and their associated coastal environments at global scales. We selected 10 rivers across three different climate zones and five continents in order to include varied levels of land surface and biological processes. Hundreds of EO-1 Hyperion images acquired from 2001 to 2011 were examined for this investigation. The two main research objectives were to: 1) assess the variations in relative CDOM levels in coastal and riverine areas from the ten study sites derived from Hyperion data and the QAA-CDOM algorithm, and 2) investigate the potential of Hyperion imagery and the QAA-CDOM algorithm to detect CDOM seasonal variation at the same 10 locations. The investigation focused on five aspects of CDOM in riverine and estuarine systems: 1) the range of worldwide CDOM levels, 2) spatial distribution patterns, (3) climatic influences, (4) influences of landuse change, and (5) seasonal effects.

Unlike many studies that address global scale phenomena, our use of Hyperion imagery took advantage of the relatively high spectral (i.e. 10 nm wide bands) and spatial (i.e. 30 m) resolution of this platform, while also providing scientific insight of scenarios responsive to global scale climatic and environmental variables. The CDOM dynamics of the near-shore/river interface are applicable to a variety of research topics and to the management of coastal environments. Specifically, CDOM dynamics can help to better understand DOC export processes from terrestrial inputs/carbon sinks to coastal waters as part of the carbon cycle.

2. Methods

2.1. Study sites

The 10 major rivers from five continents selected for this study are the: Mississippi River and Mackenzie River in North America, Amazon River and Plata River (Rio de la Plata) in South America, Yangtze River (Changjiang) and Irrawaddy River in Asia, Nile River and Congo River in Africa, and Rhine River and Volga River in Europe. They are all well-known major rivers with large drainage areas and significant discharge, playing a crucial role in the hydrologic systems of each continent. All are closely linked to the human populations along their shores, serving functions such as water supply, agricultural irrigation and transportation corridors. They drain and traverse varied and diverse ecosystems, such as arid desert (i.e. lower Nile River), humid tropical forests (i.e. upper Nile River), tropical evergreen forest (i.e. Amazon River) and boreal forest (i.e. Mackenzie River). These big rivers typically deposit large alluvial fans (i.e. deltas) where they flow into their estuarine and coastal regions. Often, as in the case of the Nile River and Yangtze River Delta, high human population densities are supported on these deltaic sediments. Due to the amount of discharge and sediment load, many of these rivers form huge sediment plumes at their termination, such as the Amazon River and Mississippi River. Some of the selected rivers periodically freeze, such as the Mackenzie River and Volga River. The general characteristics of each river, including the length, watershed area, annual discharge, outflow, and climate type, are listed in Table 1. The relative locations of the 10 rivers used in this study are shown on a world map (Fig. 1).

Data obtained or collected from ten additional estuarine and coastal locations along with the Mississippi River and Amazon River study sites outlined above were used for algorithm validation. The ten additional sites are; the Atchafalaya River in Louisiana, the Passaic River, Hackensack River, and Newark Bay in New Jersey, the Hudson River along the New Jersey/New York border, the Neponset River and Boston Harbor in Massachusetts, the Saginaw River and Kawkawlin River in Michigan, and the Brisbane/Logan/Pine/Caboulture Rivers flowing into Moreton Bay in Australia (Brando & Dekker, 2003). As outlined in Table 2, the Amazon River and Moreton Bay validation data were extracted from previous studies (Brando & Dekker, 2003; Zhu & Yu, 2013), while data collected in the United States were derived from our in-situ measurements. The in-situ data used to derive relative CDOM levels were measured below water surface at relatively high spatial resolution (i.e. 5 m intervals) with concurrent R_{rs} (remotely sensed reflectance) measured just above the water surface. These in-situ data below and above water surface were collected through our multiple research cruises in rivers in Louisiana, New York, and Massachusetts. Recently, we also conducted several research cruises in freshwater environments and validated the algorithm for the Saginaw River, Kawkawlin River, and the Lake Huron in Michigan. The rivers used for the validation are latitudinally well distributed across the continental U.S. (Table 2).

2.2. Hyperion imagery

In November of 2000, NASA launched the Earth Observing-1 satellite mission as part of their New Millennium Program, with the Hyperion imaging spectrometer being a key component of this mission.

Table 1
Hydrological properties of the ten studied rivers.

River	Rank*	Outflow	Length (km)	Discharge (10^3 m^3/s)	Drainage area (10^3 km^3)	Climate categories
Mississippi	1st, N. Am.	Gulf of Mexico	5971	17.30	3220	Subtropical
Mackenzie	2nd, N. Am.	Beaufort Sea	4241	7.93	1805	Frigid
Amazon	1st, S. Am.	S. Atlantic Ocean	6400	212.38	5778	Tropical
Plata	2nd, S. Am.	Rio de la Plata	4880	14.89	2305	Subtropical
Yangtze	1st, Asia	East China Sea	6300	21.80	1942	Subtropical
Irrawaddy	23rd, Asia	Andaman Sea	1992	13.56	430	Tropical
Nile	1st, Africa	Mediterranean Sea	6650	2.83	2978	Subtropical
Congo	2nd, Africa	S. Atlantic Ocean	4700	39.64	4014	Tropical
Volga	1st, Europe	Caspian Sea	3530	8.06	1380	Temperate
Rhine	15th, Europe	North Sea	1392	2.21	145	Temperate

* The rank is by river's length. The data of length, discharge, and drainage area are from *The Water Encyclopedia*, 3rd Ed., by Pedro Fierro, Jr. and Evan K. Nyer.

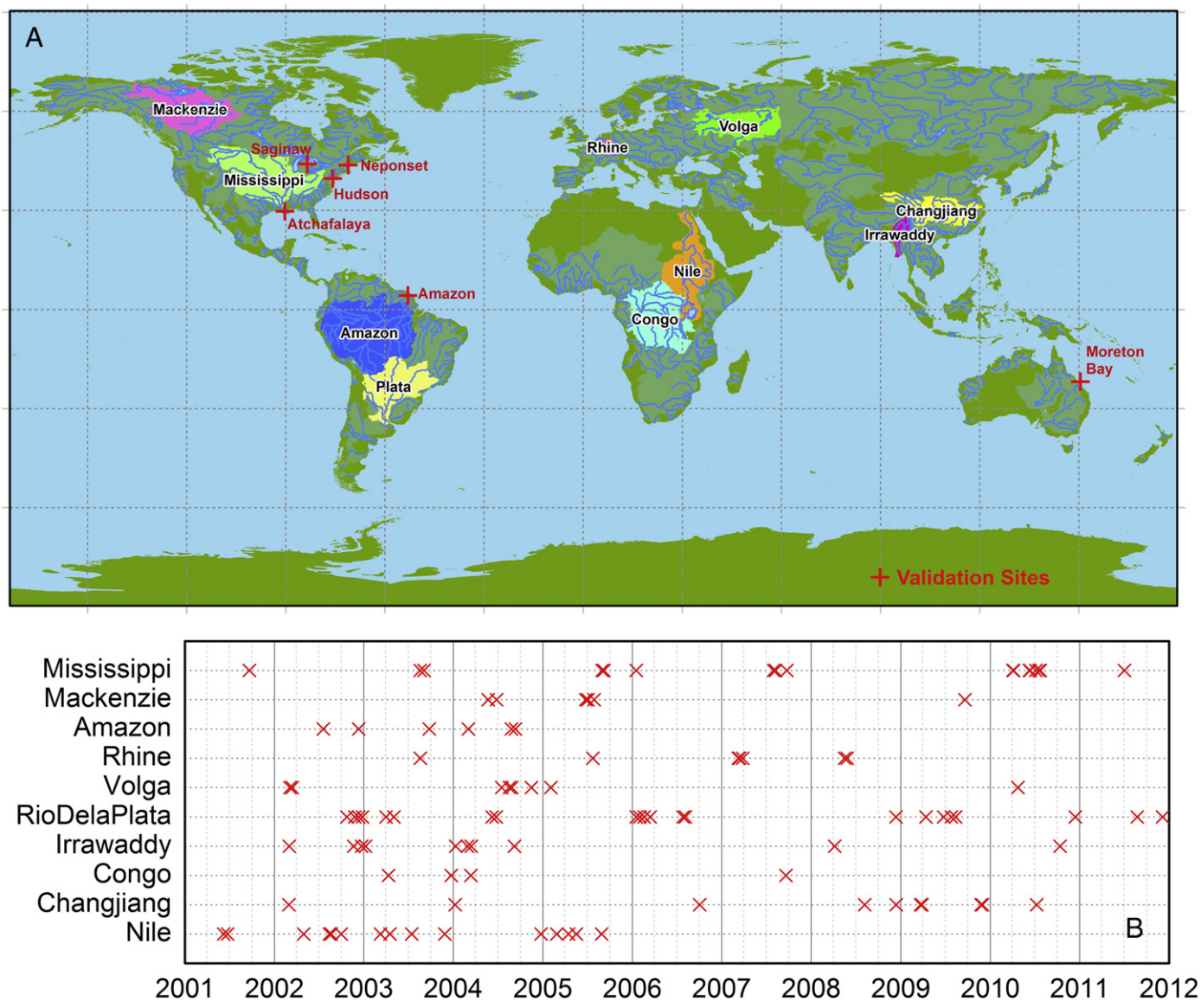

Fig. 1. (a) Study site map of 10 global major rivers and their watersheds and 6 estuarine and coastal regions for validations. (b) The acquisition dates of available EO-1 Hyperion images of each river.

Hyperion has the following characteristics: 220 bands, each being 10 nm in width, spectral range from 400 to 2500 nm, swath width of 7.5 km and typical swath length of 42 km, 30 m GSD and 12 bit image data.

Hundreds of Hyperion images were available in total for the 10 rivers (Fig. 1) included in this study, from a multitude of overpass dates displaying varied atmospheric conditions. As an example, Fig. 2a shows the nineteen 7.5 km wide, Hyperion image swaths

Table 2
Validations of QAA-CDOM. The Amazon's data were from the products of the Coast Colour Project (http://www.coastcolour.org/site_21.html), Moreton Bay's data were from Brando and Dekker (2003), and all others were from our in situ measurements.

River, bay, lake	Location	RMSE m^{-1}	AME %	Measured $a_g(440)$ m^{-1}			Derived $a_g(440)$ m^{-1}		
				Min	Mean	Max	Min	Mean	Max
Mississippi	Louisiana, USA	0.16	27	0.07	0.11	0.60	0.04	0.08	0.40
Amazon	Brazil	–	11	–	3.80	–	1.80	4.20	8.60
Atchafalaya	Louisiana, USA	0.12	14	0.80	1.62	3.60	0.60	1.40	4.00
Moreton Bay	Australia	–	–	0.13	–	0.75	0.15	0.45	0.80
Hudson	New York, USA	0.45	63	0.41	0.75	0.87	0.13	0.28	0.68
Hackensack	New York, USA	0.21	16	0.94	1.16	1.43	0.17	1.35	3.01
Passaic	New York, USA	0.15	17	1.01	1.28	1.42	0.58	1.06	1.96
Newark Bay	New York, USA	0.17	43	0.75	0.80	0.87	0.72	1.14	1.95
Neponset	Massachusetts, USA	0.43	52	0.57	0.98	1.53	0.09	0.47	1.42
Saginaw	Michigan, USA	0.25	19	0.17	1.94	3.66	0.42	2.31	7.76
Kawkawlin	Michigan, USA	0.38	3	0.12	2.07	8.46	0.14	2.00	8.04
Lake Huron	Michigan, USA	0.37	27	0.11	0.84	1.82	0.16	0.61	1.89

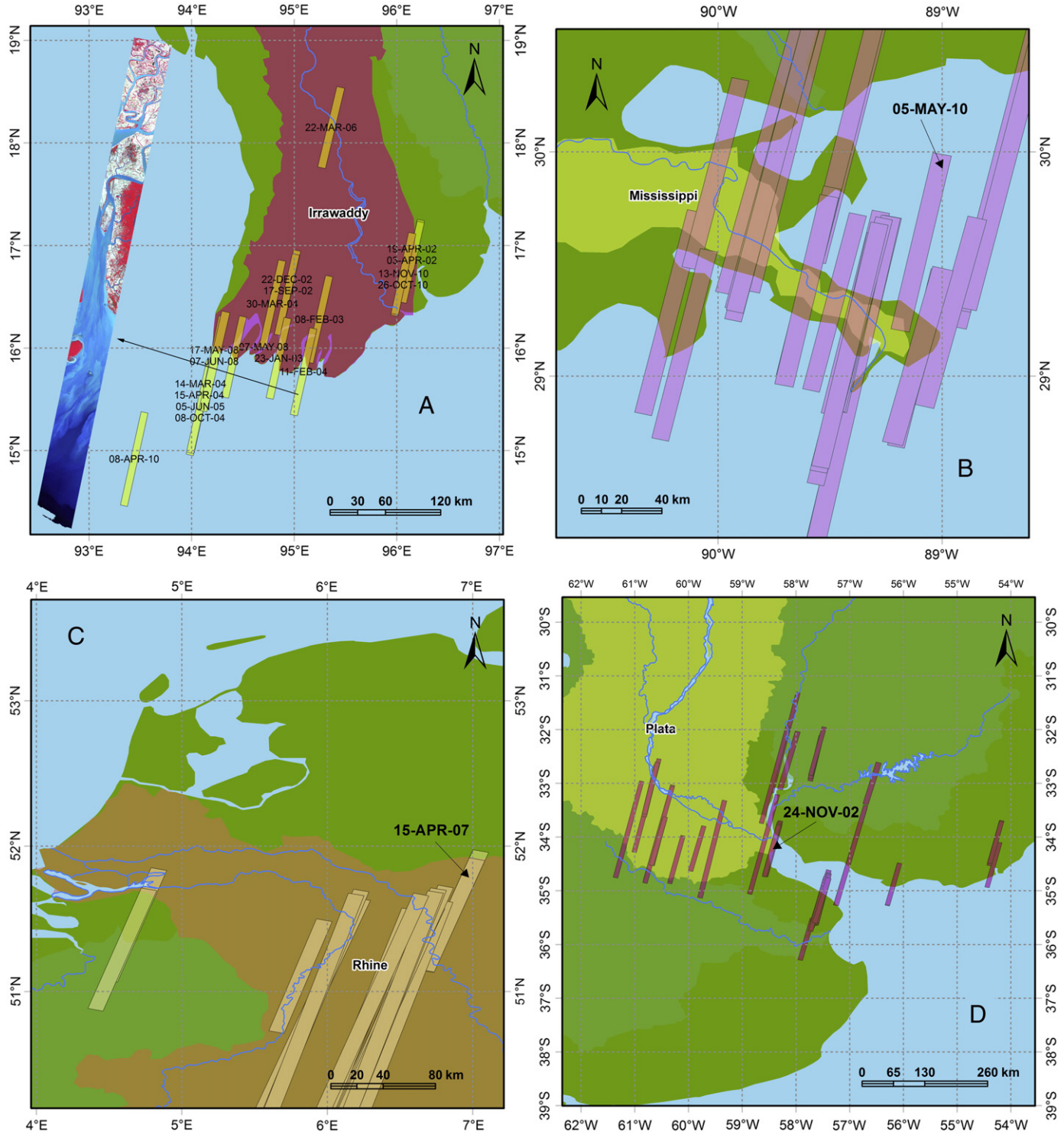

Fig. 2. (a) The Irrawaddy River Delta and the locations and dates of EO-1 Hyperion images covering this region (an example raw image was acquired on 02/11/2004). (b), (c), (d) are similar cases for the Mississippi River, Rhine River, and Plate River, respectively. The images labeled with dates are those used as the examples shown in Table 3.

available of the Irrawaddy River. Fig. 2a also shows, in more detail, a single swath capturing a portion of the Irrawaddy River estuary, ranging from the river channel in the northeast to offshore saline water in the southwest, acquired on 02/11/2004. Fig. 2b, c, and d shows the similar examples in other three rivers: the Mississippi River, Rhine River, and Plata River. As expected, the available imagery displayed varied atmospheric conditions and cloud coverage, which ultimately led to selecting a subset of high quality Hyperion images for each river.

2.3. QAA-CDOM algorithm

The QAA-CDOM algorithm is used for the extraction of $a_g(440)$, the CDOM absorption coefficient at 440 nm, from remote sensing reflectance R_{rs}. The algorithm was introduced by Zhu & Yu (2013) and Zhu et al. (2011) for extracting riverine and estuarine CDOM. The QAA-CDOM was an improvement of the QAA algorithm developed earlier by Lee et al. (2002, 2007). Unlike the QAA algorithm, the QAA-CDOM algorithm calculates CDOM absorption in two major

steps. The first step is to derive the total adsorption coefficient $a_t(440)$ and the backscattering coefficient $b_{bp}(555)$ from suspended particulate matter at a wavelength of 555 nm by optimizing the QAA algorithm (Lee et al., 2002; Zhu & Yu, 2013). The QAA algorithm requires remote sensing reflectance at 4 wavelengths (440, 490, 555, and 640 nm) as inputs to reduce errors caused by the interference from chlorophyll and other plant pigments in natural waters. The second step is to use an our previously extended QAA algorithm (QAA-E) to derive the absorption coefficients of phytoplankton and non-algal particles $a_p(440)$ calculated with Eq. (1) below (Zhu et al., 2011). The value combined with the total adsorption coefficient $a_t(440)$ was used to generate $a_g(440)$ via Eq. (2).

$$a_p(440) = j_1 b_{bp}(555)^{j2} \quad (1)$$

$$a_g(440) = a_t(440) - a_p(440) \quad (2)$$

where j_1 and j_2, are two parameters that were estimated from all available synthetic and in-situ data for both open-sea and coastal waters.

2.4. Field measurements and image preprocessing

Field measurements for validating the QAA-CDOM algorithm were acquired from August 24–30, 2007, of the Mississippi River plume. We measured continuous underwater attenuation and absorption coefficients, salinity, CDOM fluorescence, chlorophyll fluorescence, and optical backscattering for suspended sediments by using a towed undulating vehicle (ECOShuttle). At the same time of underwater measurements, above-surface hyperspectral measurements were completed via a portable spectroradiometer (ASD FieldSpec®). Discrete water samples were also collected every half hour and analyzed in order to calibrate field instrumentation. The speed at which the ECOshuttle was towed resulted in a sampling interval that equated to a measurement being taken approximately every 1 m, which ultimately created an extremely large dataset containing approximately 1,000,000 underwater measurements. In addition, approximately 20,000 above-surface spectra and 150 discrete water samples were collected. Similar measurement campaigns were also carried out in Hudson River regions on October 23–25, 2006 and July 28–August 7, 2010, in Neponset River regions on September 25 and November 04, 2009, and in Saginaw River regions on May 10 and October 18, 2012.

The EO-1 Hyperion satellite images were retrieved from the United States Geological Service (USGS, http://earthexplorer.usgs.gov/). For each study site, we selected 4–10 higher quality images by considering relative location of the study site within the larger image, capture date and cloud conditions. Each image was pre-processed by replacing missing lines, de-striping, and de-noising. The atmospheric correction was carried out by the FLAASH module provided by ENVI 4.8. R_{rs} was obtained by removing the surface reflectance (Zhu & Yu, 2013). The positional, atmospheric, and weather parameters (i.e. satellite looking angle, sun elevation, wind speed, humidity, and visibility) required by atmospheric correction and surface correction were retrieved from image metadata and the National Climatic Data Center (NCDC) weather database.

2.5. Determining CDOM concentration for the 10 rivers and validation methods

Relative CDOM concentrations, $a_g(440)$, derived from the QAA-CDOM algorithm can vary greatly within an image scene. This should be expected considering the spatial variability of the imagery, with a single scene that could vary from an inland river corridor to Case 1 water in open seas. We assumed that four different CDOM output parameters gleaned from the QAA-CDOM algorithm were pertinent to this investigation: $CDOM_{median}$, $CDOM_{max}$, $CDOM_{min}$ and relative freshwater relative CDOM level ($CDOM_{fresh}$). The minimum and maximum CDOM values were computed by averaging the lowest 5% and highest 5% CDOM levels found across all of the water pixels, respectively. To determine $CDOM_{fresh}$, we extracted output values from randomly selected pixels falling near the midstream of the freshwater headwaters as far from the river mouth as possible. The annual mean concentration ($CDOM_{a\text{-}fresh}$) of each river was determined by averaging $CDOM_{fresh}$ for all applicable images and collection dates.

The reliability of the output parameters derived from the QAA-CDOM algorithm were then compared to their paired field measurements outlined in Section 2.4 in order to evaluate the validity of the algorithm. Fig. 3 shows the relationship between the derived and measured CDOM levels across all 10 locations ($R^2 = 0.81$). Both a RMSE (Root Mean Squared Error) and AME (Absolute Mean Error) were calculated by comparing the measured and derived $a_g(440)$ values for all applicable sampling locations using Eqs. (3) and (4), respectively.

$$RMSE = \sqrt{\frac{\sum_{i=1}^{n}\left[\log\left(a_g(440)_i^{derived}\right) - \log\left(a_g(440)_i^{measured}\right)^2\right]}{n-2}} \quad (3)$$

And

$$AME = \frac{\sum_{1=1}^{n}\left(\left|\frac{a_g(440)_i^{derived} - a_g(440)_i^{measured}}{a_g(440)_i^{measured}}\right|\right)}{n} \quad (4)$$

3. Results and discussion

3.1. Field validation

The validations were made by comparing the measured CDOM against the algorithm derived CDOM for the 10 validation sites in the U.S.A. We validated the algorithm derived CDOM for the Amazon River and Moreton Bay against the information in published reference

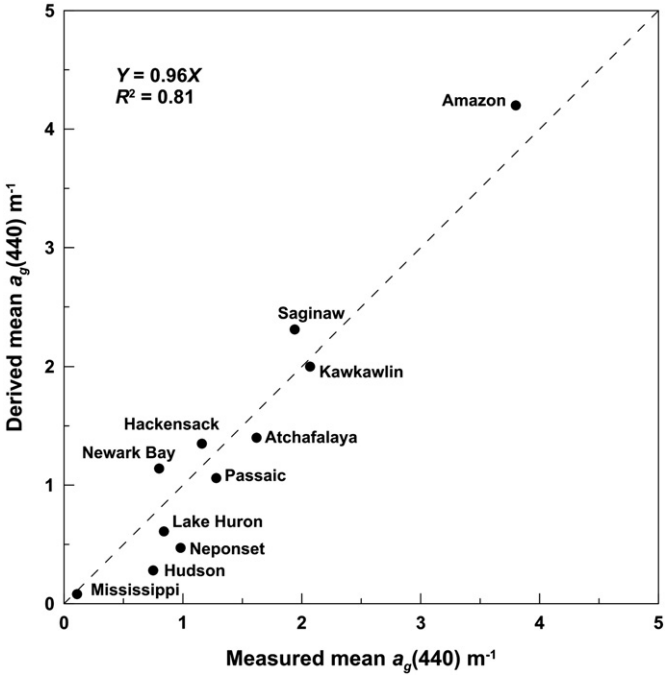

Fig. 3. Comparing the measured and derived CDOM $a_g(440)$ from 11 estuarine and coastal regions.

to see if they are in the same order of magnitude (Zhu & Yu, 2013). The overall RMSE and AME for the measured versus derived $a_g(440)$ values across all twelve validation sites are 0.269 m^{-1} and 26.5% respectively. Currently, the accuracy of relative CDOM level estimations via remote sensing based algorithms utilizing CDOM absorption coefficients in open-sea water displays an overall RMSE range of = 0.2–0.3 m^{-1} (IOCCG, 2006). As Table 2 illustrates, our validation results of the QAA-CDOM algorithm for complex estuarine and coastal waters displayed RMSE values similar to those generated from open-sea environments. Our RMSE values indicate a marked improvement over other popular CDOM algorithms when applied to complex estuarine and coastal waters. For example, the QAA-CDOM algorithm performed exceedingly well in complex freshwater environments like the Saginaw and Kawkawlin River plume regions (Zhu et al., 2012). CDOM levels estimated from in situ measurements ranged from 0.11 to 8.46 m^{-1}, while QAA-CDOM's estimation of relative CDOM levels in these two regions was 0.14–8.04 m^{-1}, with an RMSE of 0.29 m^{-1}. Overall, the similarity between in-situ and remotely derived CDOM concentrations illustrates that the QAA-CDOM algorithm has advantages in detecting broad range of CDOM concentrations in land–water interface areas as well as open-seas.

The validation results also show that the QAA-CDOM algorithm works well for different climate zones, including tropical (Amazon), subtropical (Atchafalaya, Mississippi and Moreton Bay), and temperate zones (others 8 sites in the Great Lakes, and Middle Atlantic coastal regions). For example, the AME for the Atchafalaya River and Amazon River is less than 20%. Similarly, Moreton Bay CDOM values ranged from 0.15 m^{-1} to 0.8 m^{-1},which matched well with the observed range (0.13 m^{-1}–0.75 m^{-1}). In addition, overall RMSE related to the urban regions/study sites (i.e. Boston in the Neponset River and New York City in the Hudson River region) is also satisfactory at 0.28 m^{-1}. Our extensive validation efforts indicate that the QAA-CDOM algorithm is very effective for studying CDOM levels and their spatial variation in estuaries and coastal water environments worldwide. The details about field observations have been reported in our early studies (Zhu, 2011; Zhu et al., 2012; Zhu and Yu, 2013; Zhu et al., 2011).

3.2. Minimum and maximum CDOM estimates

Table 3 lists the range of relative CDOM levels calculated for each study location. The overall minimum CDOM (0.02 m^{-1}) was observed in the Nile River in August of 2003, while the maximum (7.2 m^{-1}) was observed in the Mackenzie River in June of 2004. As expected, CDOM concentration in riverine and estuarine waters is much higher than CDOM in off-shore and open-sea waters (typically < 1 m^{-1}). Many previous in-situ measurements have confirmed that riverine and inland-water CDOM concentrations can be as high as 19.4 m^{-1} (Brezonik et al., 2005; Kowalczuk et al., 2003). Our CDOM field measurements from related investigations of several U.S. rivers (Mississippi, Atchafalaya, Hudson, Neponset, and Saginaw Rivers) ranged from as low as 0.02 m^{-1} to as high as 8.46 m^{-1}.

Table 3
CDOM concentrations derived from Hyperion images of the ten rivers (corresponding images are shown in Figs. 2, 4, 5, 9, and 11).

River	Date	Location	CDOM $a_g(440)$ m^{-1}		
			Min	Mean	Max
Mississippi	05/05/2010	Coastal regions adjacent to channel	0.08	0.30	0.58
Mackenzie	06/23/2004	Coastal regions adjacent to channel	1.79	4.35	7.20
Amazon	10/12/2004	Channel very closing to mouth	2.50	3.51	6.04
Plata	11/24/2002	River mouth	1.93	3.36	4.78
Yangtze	02/09/2004	Channel very closing to mouth	0.45	0.75	0.97
Irrawaddy	02/11/2004	Channel and plume regions	0.11	1.86	3.77
Nile	08/16/2003	Channel and plume regions	0.02	0.65	2.52
Congo	04/13/2004	Channel very closing to mouth	0.20	0.56	0.88
Volga	09/18/2004	Channel very closing to mouth	0.63	1.32	2.35
Rhine	04/15/2007	Channel closing to mouth	0.49	0.83	1.48

3.3. Spatial distribution patterns

The spatial patterns visible when relative CDOM concentrations were displayed across each image demonstrated that CDOM loading plumes and degradation processes are likely being well captured by the QAA-CDOM output (Fig. 4). Plumes with relatively high CDOM concentrations (e.g. R1-R6, R8, R11-R13) are directly adjacent to riverbanks where they are likely receiving CDOM originating from terrestrial sources (i.e. allochthonous). The locations of these QAA-CDOM generated plumes are valuable information for ecological studies because bio-optical properties of inland waters are usually complicated by the preponderance of organic matter and suspended sediment in the discharge emanating from the surrounding watersheds. The high CDOM concentrations can significantly alter water color by affecting light absorption and scattering.

The algorithm is also effective for identifying CDOM plumes that originated from areas with high concentrations of aquatic algae and plankton. For example, R7 delineates a CDOM plume near the center of the channel of the Mississippi River (Fig. 4d). The modest but detectable elevated CDOM concentrations indicated by this plume are higher than adjacent waters by approximately 0.1 m^{-1} as illustrated in its concentration profile (Fig. 6c). Because there are no significant terrestrial CDOM sources in the immediate vicinity, and flow from the outlet of a smaller tributary (see image subset in Fig. 2b for its location) is relatively low, it is assumed that the small spike in CDOM level in this mid-channel plume is due to autochthonous sources such as phytoplankton/algal blooms. The ability of remote sensing based algorithms to detect off-shore/mid-channel CDOM plumes generated from non-terrestrial sources was also observed in studies of the Gulf of Mexico (Tomlinson et al., 2004; Wynne et al., 2005).

The mapped CDOM consistently displays an inverse relationship along the salinity gradient from inland freshwater to saline ocean waters. An example that best illustrates this inverse relationship is the Irrawaddy River (Fig. 5b). Consistent with this inverse relationship, CDOM levels decrease from within the upper river tributaries to the river mouth area (Fig. 6a).

The QAA-CDOM algorithm is also sensitive to fluctuations in relative CDOM levels due to anthropogenic sources. In Fig. 5, human influences on relative CDOM levels are clearly illustrated along a particular stretch of the Nile River. In this portion of the Nile River, the profile (Fig. 6b) shows two spikes in CDOM levels, one directly downstream of the City of Damietta (R13) and one downstream of the City of Ras El Bar (R14). Such sudden CDOM increases must be attributed to urban nutrient loading. This CDOM increase (R14), was very unique across the hundreds of Hyperion images analyzed, and indeed hard to explain. It is likely that is was the result of an unknown autochthonous source, such as a CDOM bloom generated by phytoplankton or algae.

The Rhine River also illustrates the sensitivity of the QAA-CDOM algorithm to the inherent nature of the surrounding watershed (Fig. 4c). The concentration profile shown in Fig. 6d is relatively low in concentration and shows little relative variation. The landscape adjacent to this section of the Rhine River is relatively homogeneous and thus lacks significant variation in the biological and chemical processes. These data illustrate that the QAA-CDOM algorithm may be an effective tool for investigating the role local biogeography and associated land surface processes play in affecting water quality using CDOM as a surrogate measure.

3.4. Identifying climatic influence on CDOM variation

Another one component of this study was to investigate whether remote sensing is capable of identifying the climatic influence on

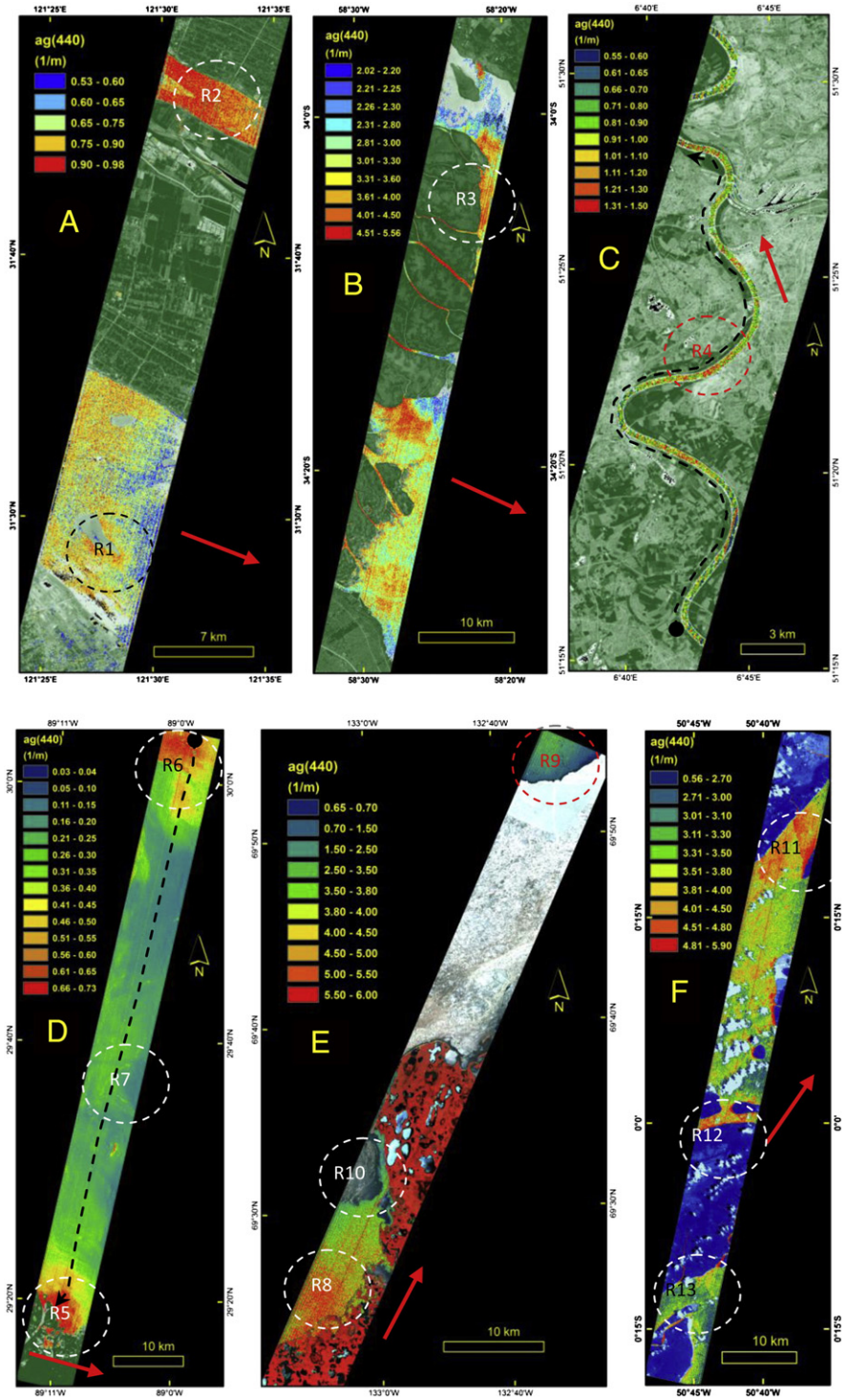

Fig. 4. CDOM levels ($a_g(440)$, m^{-1}) in estuarine and coastal regions of six rivers: (a) Yangtze, (b) Plata, (c) Rhine, (d) Mississippi, (e) Mackenzie, and (f) Amazon. The red arrows indicate the directions of river flow. The dash-circled areas are regions of interest (R#) discussed in Section 4 and the black dash lines are profile tracks shown in Fig. 6. (For interpretation of the references to color in this figure legend, the reader is referred to the web version of the article.)

CDOM variation. Since a large river watershed could span across multiple climate zones, we indicate climate effects by using a very broad categories: Tropical, Sub-tropical, Temperate and Frigid climates for the estuarine and coastal regions of the ten river watersheds (see Table 1). The primary focus is on two linked climate variables: temperature and precipitation. Fig. 7a shows that $CDOM_a$ concentrations generally decrease across each of four climates from the Tropical (Amazon, 3.55 m^{-1}) to Temperate (Rhine, 0.86 m^{-1}). The trend is more pronounced when we calculated CDOM levels to averages for each climatic category as illustrated in Fig. 7b. These results illustrate that the QAA-CDOM algorithm may have the potential to identify CDOM variations influenced by climate, although it may be difficult to systematically isolate this variation from other influencing variables. It should be noted that the analysis of impacts of climate on riverine CDOM levels presented here were derived from only a few representative images acquired across varied calendar dates and

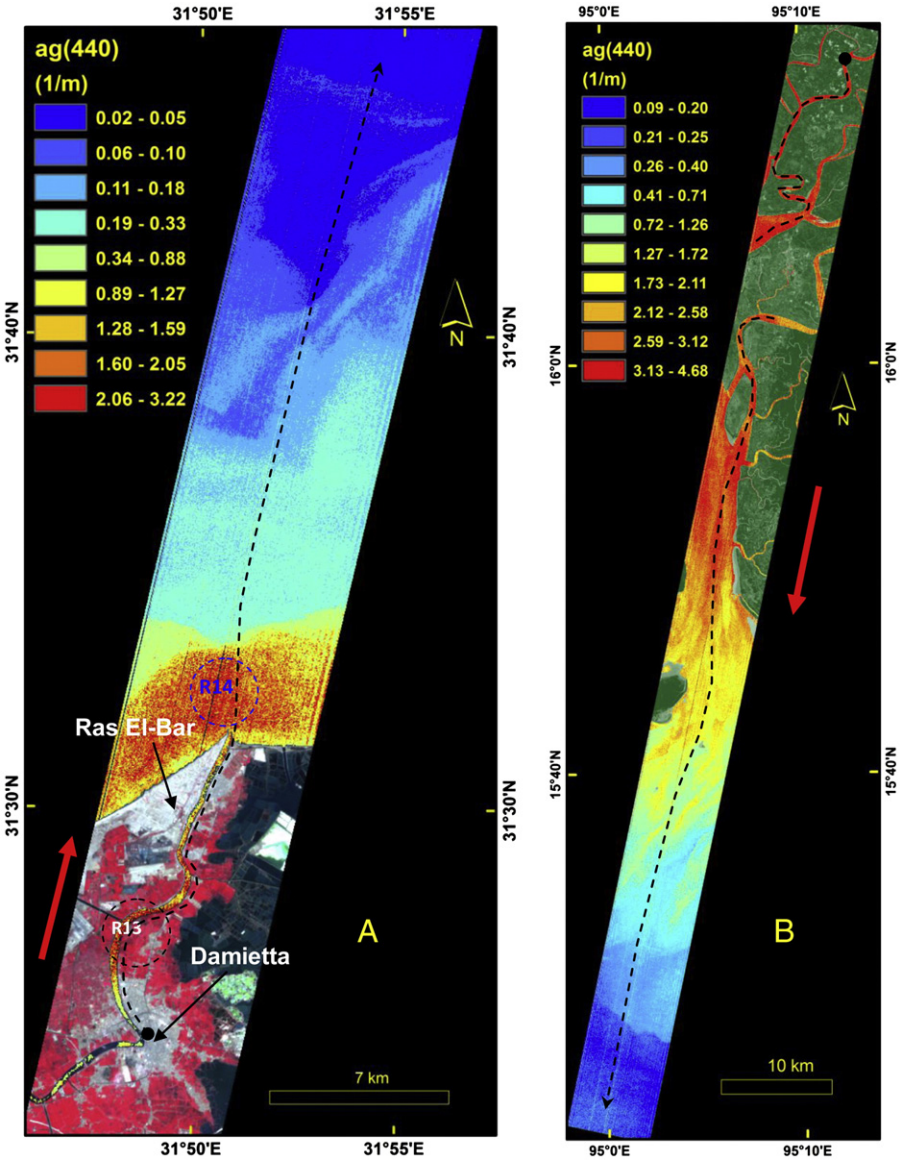

Fig. 5. Spatial distributions of CDOM levels ($a_g(440)$, m^{-1}) in estuarine and coastal regions of (a) Nile River and (b) Irrawaddy River, collected on 08/16/2003 and 02/11/2004, respectively.

years. The inherent variability of river CDOM concentrations, which is as largely determined by the annual and seasonal variations in the biological and chemical processes of the surrounding watershed, may be greater than the differences attributable to climate alone as illustrated by the Mackenzie River.

The Mackenzie River, the only studied river in frigid climate, displayed the highest CDOM level (4.51 m^{-1}; Fig. 7a). It has been reported that the Mackenzie River typically has a relatively high biochemical load (e.g. CDOM), especially during the compressed summer season (a year in Frigid Zone can be divided into two seasons: long winter and a short and active summer) at these latitudes (Retamal et al., 2008). The CDOM levels calculated by the QAA-CDOM algorithm for the Mackenzie River were extracted from a summer image, and one would expect the annual mean CDOM concentration, that would include the less productive winter months, to be significantly lower. However, it is also possible that the maximum CDOM concentration could occur during early summer/late spring. Some previous research (Kutser, 2012; Retamal et al., 2007) explained that the high CDOM concentrations in rivers and lakes in the frigid climate might be attributable to a prolonged period of snow melt resulting in a short term increase in soil carbon. During winter periods, ice breaks down cells of peat and other organic material in permafrost and water from precipitation and snow melt washes the carbon into rivers, thaw ponds and lakes during the warm period. Preliminary results reported (Tian et al., 2012) that overall climate zone and linked precipitation amounts (rain, snow, ice melting, and glacial runoff) do indeed affect riverine CDOM. A large number of ice/snow areas (white regions) are visible in the Mackenzie River Hyperion scene as shown in Fig. 4e, and the CDOM concentration in waters adjacent to these ice/snow margins were elevated and ranged from1.6 m^{-1} (R8) to 2.73 m^{-1}(R9). This scenario indicates that ice/snowmelt does indeed tend to affect ambient CDOM, which is also consistent with previous reports in the arctic and boreal regions (Dyson et al., 2011).

3.5. Influence of biogeography on CDOM variations at a global scale

Many studies have outlined that the most significant source of riverine CDOM comes from surrounding terrestrial sources, largely decaying plant material/detritus in inland tributaries/streams or soil

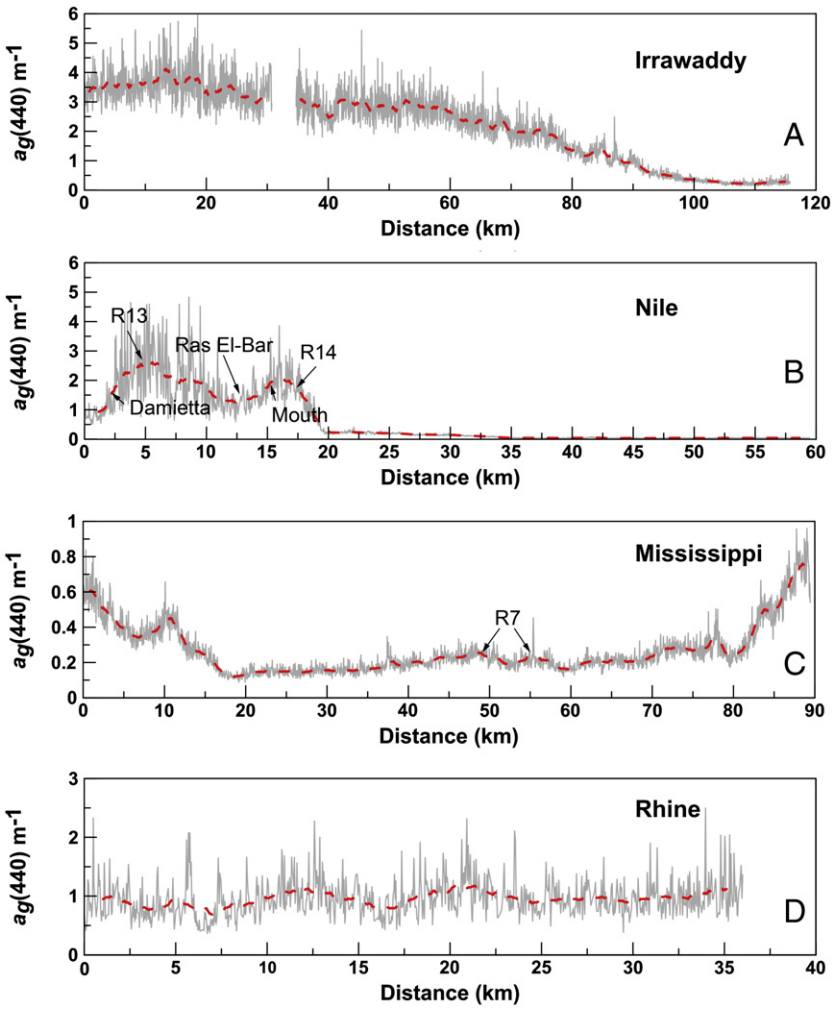

Fig. 6. CDOM level profiles of four rivers: (a) Irrawaddy, (b) Nile, (c) Mississippi, and (d) Rhine. Their tracks are shown in Figs. 4 and 5. The distance is calculated from the start point (the circle end of track line) in each image.

leachates transferred into rivers by surface or ground water runoff (Gardner et al., 2005). Thus, land-cover/bio-geophysical variables, such as gross biomass, vegetation density, soil type, and land-cover, play a documented and important role in determining CDOM concentrations (Tian et al., 2012). In order to investigate how sensitive the QAA-CDOM algorithm is to the influence of select biophysical variables, overall percent forest cover of each watershed was obtained from the Global Land Cover Classification database created by the

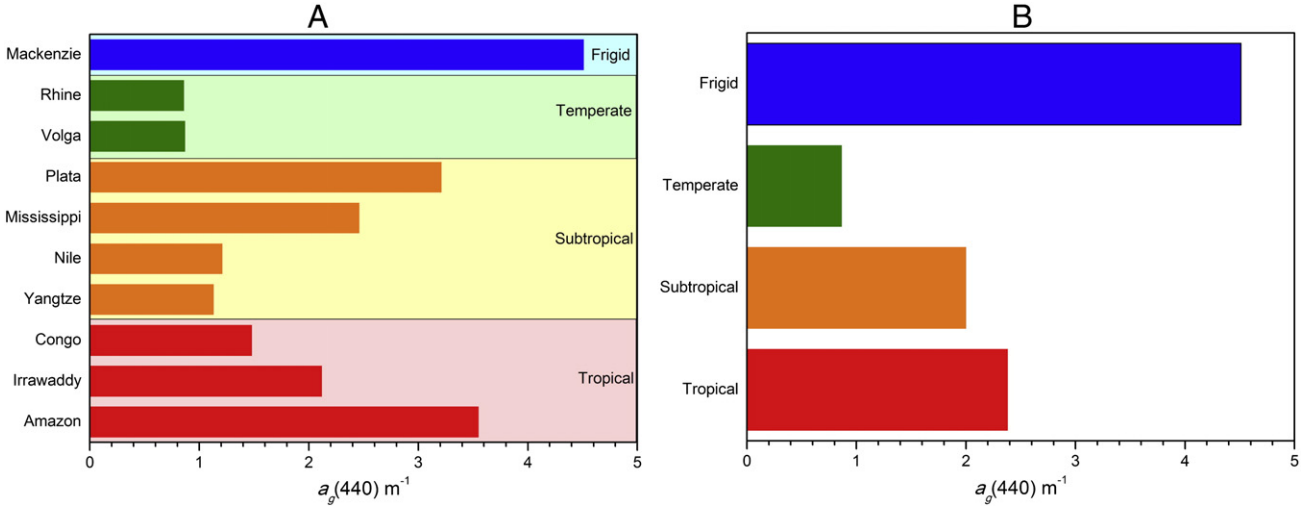

Fig. 7. (a) Riverine and estuarine $CDOM_a$ for the rivers falling within the four climate zones, (b) average $CDOM_a$ among the rivers falling within the four climate categories.

University of Maryland. Using these landcover data, we categorized the 10 study rivers into three groups based on their percent forest coverage as follows: 0%–30% (i.e. Nile, Yangtze, Plata, Rhine, and Mississippi), 30%–60% (i.e. Volga, Irrawaddy, Mackenzie, and Congo), and 60%–90% (i.e. Amazon). Average CDOM concentrations were plotted against these forest cover percentages in Fig. 8, As expected, the average CDOM levels throughout the entire watershed steadily increased as the percent forest coverage increased; 0%–30% (1.77 m^{-1}), 30%–60% (2.24 m^{-1}) and 60%–90% (3.55 m^{-1}). The QAA-CDOM algorithm seems capable of detecting relative CDOM levels attributable to gross watershed forest cover.

It is important to note that the relative locations of the forested areas within the overall watershed will significantly influence the variation of riverine CDOM levels. For example, if the majority of the forest cover is concentrated in the most downstream portions of the watershed, one would expect the terrestrial input of these forests to have a more significant effect on river mouth CDOM levels due to their relative proximity. This investigation does not present enough data or did not include an analysis that attempted to identify how the spatial distribution of the forested areas within the overall watershed influences CDOM levels. However, this represents a promising topic for future research.

Further trends were identified when the relationship between relative CDOM levels and the percentage of different land cover types within the watershed were compared. The percentage of deciduous broadleaf forest coverage within an individual watershed, among rivers grouped according to their climate zone, may become the dominant determinant of relative CDOM levels. For example, Fig. 7a shows that subtropical $CDOM_a$ values in the Plata and Mississippi Rivers mouths were much higher than that of the Yangtze and Nile Rivers. This marked difference in average CDOM levels across these four rivers was attributed to the relative percentage of deciduous broadleaf forest cover within each watershed (i.e. Mississippi 9.4%, ranks 1st of the 10 rivers; Plata, 4.4%, 3rd, Yangtze 1.6%, 7th; Nile 0.1%, 10th). It seems likely that the higher $CDOM_a$ levels were attributable to the relatively high levels of deciduous broadleaf forest cover, which in turn result in higher carbon loads via the decay of fallen leaves. Soil type, which is clearly correlated with the percentage of overall forest cover as well as percentage of deciduous broadleaf forest, is also a plausible factor which may significantly affect relative CDOM levels and its distribution. CDOM released from soil is also a function of soil moisture and hence precipitation and thaw events.

The clear relationship between relative CDOM levels determined via the QAA-CDOM algorithm and overall forest cover within the watershed as well as relative deciduous broadleaf forest percentage speaks to the utility of this algorithm. Further research is needed that couples detailed field observations of physical variables (e.g. soil properties, hydrological characteristics and land cover) and their influence on CDOM pathways into river systems.

3.6. Seasonal CDOM variations

The CDOM levels derived from the QAA-CDOM algorithm for the Volga River showed a clear seasonal variation. This result supports recent work conducted in the Michigan waters of Lake Huron (i.e. Saginaw Bay) and the lower Saginaw River, where it was demonstrated that QAA-CDOM is able to assess seasonal CDOM variations (Zhu et al., 2012). The five images shown in Fig. 9 of the river mouth area of the Volga River were acquired in August 2004, September 2004 (2), December 2004 and March 2005. The five images clearly showed seasonal variation as illustrated by the presence of a large vegetated area as seen in the August and September scenes. The same area in the image acquired in December (winter) is displayed as bare soil (e.g. tilled agricultural fields) or senesced vegetation (e.g. agricultural residue, defoliated woody vegetation). As typical with a CIR false color composite, areas of photosynthetically active vegetation are displayed as reddish areas (i.e. Fig. 9a, b, c) while the same areas appear brown in Fig. 9d. In the March image, much of the land was snow covered (Fig. 9e). Correspondingly, the predicted CDOM levels were higher during the vegetated summer and fall (0.5–2 m^{-1}) and lower during the senesced winter and spring (0.05–0.5 m^{-1}).

The QAA-CDOM algorithm was also able to detect the influence of a significant individual rainfall event within a river. Volga River CDOM levels were calculated to be 1.3 m^{-1} on September 18, 2004, which dropped dramatically to 0.4 m^{-1} by September 27, 2004 (Fig. 10). The sharp reduction in CDOM levels was associated with the dilution effect of a moderate rainfall event (3.1 mm) on day 24 according to precipitation data recorded at three surrounding locations. It is likely that it had an increased riverine CDOM levels immediately after this modest rainfall event. Riverine CDOM levels should decrease to a lower level a few days after a rainfall event due to a reduction in soil leachates. The CDOM should increase to a higher level through respiration processes before next rainfall event. The timing of occurrences of CDOM increases and decreases are the function of rainfall intensity, rainfall duration, and drainage area affected (Tian et al., 2012). Our results suggest that the QAA-CDOM algorithm is indeed capable of monitoring relative CDOM differences resulting from within season precipitation events.

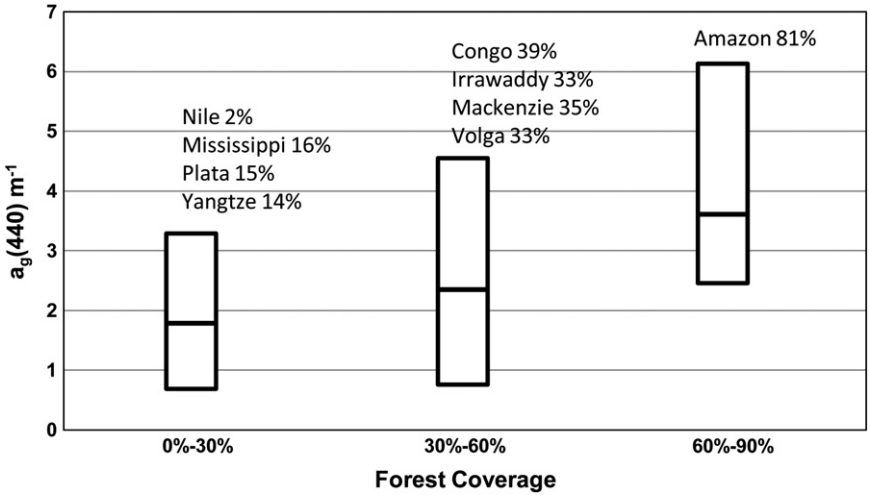

Fig. 8. Relationship between estuarine $CDOM_a$ ranges and watershed forest coverage (%). The land cover data are provided by the UMD AVHRR Global Land Cover Classification.

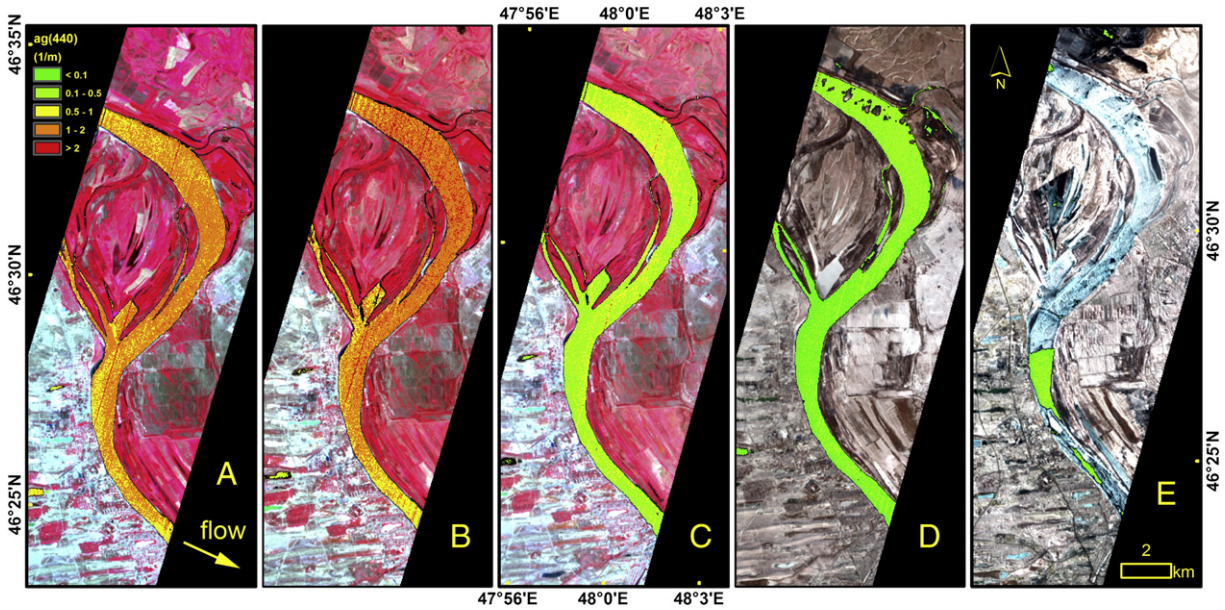

Fig. 9. CDOM levels near the Volga River mouth from various dates: (a) 08/17/2004, (b) 09/18/2004, (c) 09/27/2004, (d) 12/16/2004, and (e) 03/06/2005.

Multiple images of the Congo River were also available across different seasons at a single location. This scenario allowed us to evaluate the QAA-CDOM for rivers without clear seasonal changes. Due to its tropical climate, the Congo River does not experience significant seasonal change and most of its watershed vegetation is evergreen rain forest. The Congo River climate is characterized by frequent but localized rainfall events spawned from transient thunderstorms. The CDOM variations in the Congo River are mainly associated with these localized but heavy rainfall events (Fig. 11). For example, CDOM concentrations in January (3.5 m^{-1}) were 7–10 time higher, than that in the other months of the same season. Typically, January in this region has the highest number of transient rainfall events, which is clearly reflected in the CDOM values. Since the distribution of thunderstorms is relatively random, CDOM spatial distribution patterns in the Congo River are highly varied (Fig. 11).

3.7. Potential sensors working with the QAA-CDOM algorithm

QAA-CDOM has the potential to perform well using imagery captured from other sensors, such as the MODIS, MERIS, and SeaWiFS, since they acquire reflectance across or near the 4 required wavelengths (440, 490, 555, and 640 nm). However, the broader bandwidth and more coarse spatial resolutions captured by these sensors, it remains uncertain if the QAA-CDOM algorithm is directly applicable to various sensors. For example, SeaWiFS has an average bandwidth of approximately 20 nm, which is twice as wide as the 10 nm bandwidth of the Hyperion sensor Although it is true that the MODIS and MERIS sensors do indeed have identical bandwidths across the 4 required wavelengths, their spatial resolutions are ranged from 260 to 1000 m as compared to the 30 m resolution of Hyperion. The larger spatial resolution would result in a reduction in pixel homogeneity with these often spatially complex estuarine and coastal waters, and introduce significant error.

In the future, the QAA algorithm may be applicable to newly developed sensors and/or platforms (Worldview2, LDCM Landsat 8 and HyspIRI). Worldview2 and Landsat 8 are proposed to be multispectral sensors with the required 4 bands for QAA-CDOM as well as having a nominal spatial resolution of 30 m. The HyspIRI has all the spectral and spatial characteristics as that of Hyperion.

4. Conclusions

This study allows us to make four conclusions. First, our results indicate that the QAA-CDOM algorithm in combination with Hyperion imagery has the potential to assess a broad range of relative CDOM levels/variations (0.02–7.2 m^{-1}) as demonstrated across 10 major global rivers. This is significant because only through remote sensing applications will we be able to routinely monitor changes to rivers and their estuaries across a broad range of scales.

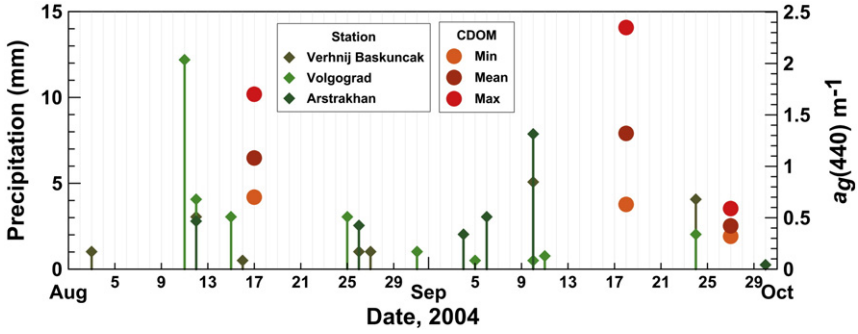

Fig. 10. Precipitation (mm) recorded and CDOM variations (a_g(440), m^{-1}) derived in the estuarine regions of the Volga River.

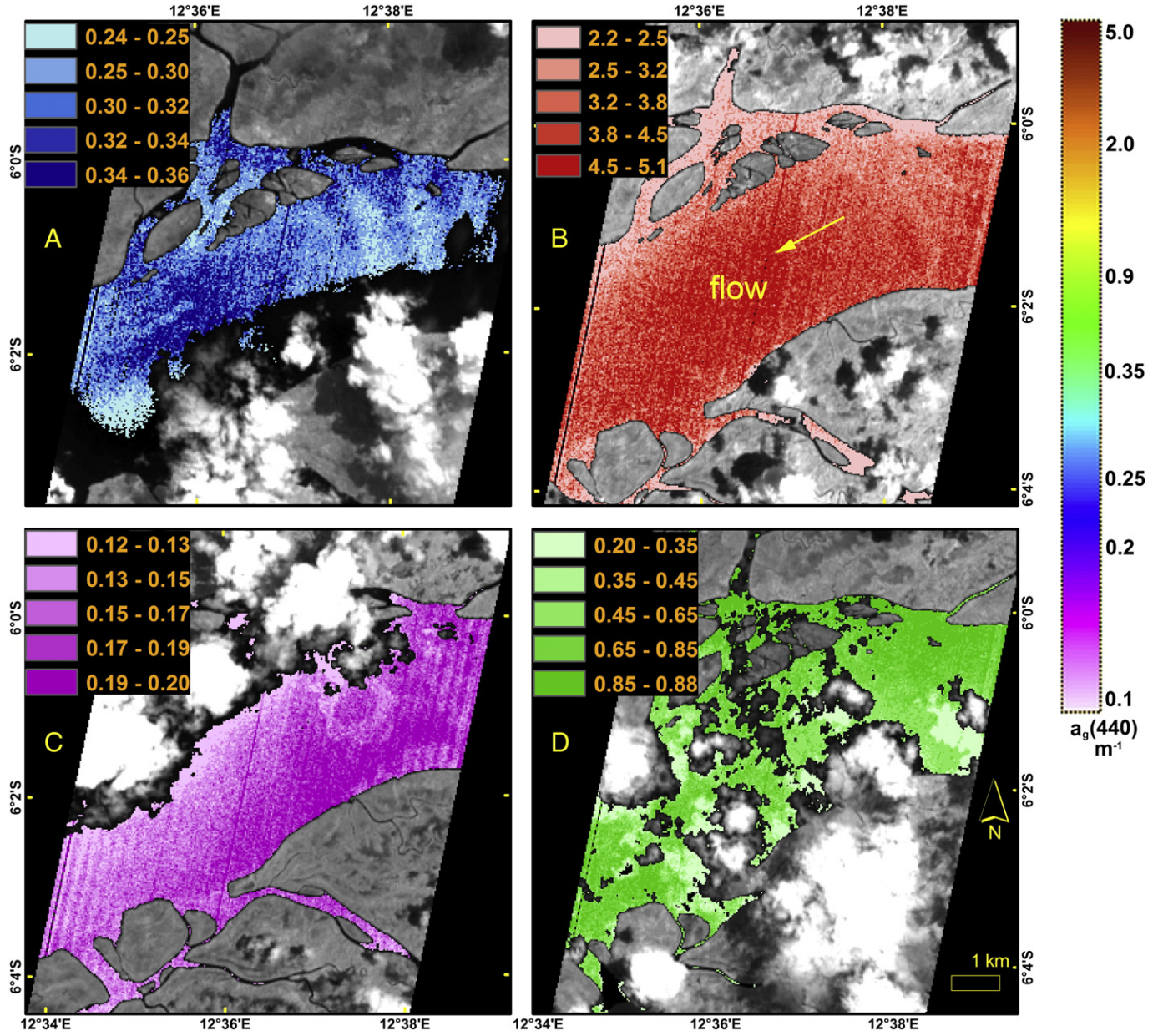

Fig. 11. CDOM levels in Congo River's channel. The four images were acquired at the same location (center: −6.027726, 12.606468) but different dates (a) 05/13/2003, (b) 01/24/2004, (c) 10/21/2007, and (d) 04/13/2004. The gray pixels were lands, clouds, or shadows.

Second, the QAA-CDOM algorithm is able to effectively delineate CDOM spatial distribution patterns within rivers at global scales. This remote sensing technology can not only be applied to the detection of riverine and estuarine CDOM plumes, but also the identification of allochthonous and autochthonous CDOM sources, which will ultimately increase our understanding of riverine carbon cycle phenomena at global/regional scales.

Third, our results suggest that the QAA-CDOM algorithm can contribute to our growing understanding of how climatic factors influence CDOM variations. This is made evident by the general trend that annual CDOM yield decreases as the climate shifts from equatorial regions to higher latitudes. Generally, seasonal CDOM variations are more significant in temperate rivers than in tropical rivers, but tropical rivers are subject to short-term temporal CDOM changes largely due to transient, episodic rainfall events.

Last, our results suggest that the QAA-CDOM algorithm is sensitive to CDOM variation resulting from watershed spatial characteristics and land cover differences, as made evident by the relationship between the model outputs with the percentage of forest coverage. More work clearly needs to be done to test the performance of the model across a wider range of watershed characteristics and land cover types.

In summary, our research confirms that it is indeed possible and likely more accurate to estimate relative CDOM levels via an algorithm that separates CDOM and sediment absorption coefficients. Overall, we are encouraged by the ability of the QAA-CDOM algorithm to extract a broad range of CDOM concentrations in rivers and estuaries worldwide, which ultimately will lead to better monitoring of land–water dynamics and environmental change at global/regional scales. The reliability and applicability of the QAA-CDOM and similar algorithms will only increase as data extracted from more detailed field measurements of biophysical parameters are verified against model output worldwide. The outcome of this research marks yet another step toward our ultimate goal to gain a better understanding

of land–water dynamics through coupling both terrestrial and water-based carbon cycling models via remote sensing methodologies.

Acknowledgment

The study was partially supported by an internal grant from Central Michigan University and two collaborative grants from the National Science Foundation (Grant #: 1025547; Grant #: 1230261). The authors would like to thank the three anonymous reviewers for their valuable comments and suggestions that improve the quality of the paper substantially.

References

Brando, V. E., & Dekker, A. G. (2003). Satellite hyperspectral remote senseing for estimating estuarine and coastal water quality. *IEEE Transactions on Geoscience and Remote Sensing*, *41*, 1378–1387.

Brezonik, P., Menken, K. D., & Bauer, M. (2005). Landsat-based remote sensing of lake water quality characteristics, including chlorophyll and colored dissolved organic matter (CDOM). *Lake and Reservoir Management*, *21*, 373–382.

Coble, P. G. (1996). Characterization of marine and terrestrial DOM in seawater using excitation emission matrix spectroscopy. *Marine Chemistry*, *51*, 325–346.

De Souza Sierra, M. M., Donard, O. F. X., Lamotte, M., Belin, C., & Ewald, M. (1994). Fluorescence spectroscopy of coastal and marine waters. *Marine Chemistry*, *47*, 127–144.

Dyson, K. E., Billett, M. F., Dinsmore, K. J., Harvey, F., Thomson, A. M., Piirainen, S., et al. (2011). Release of aquatic carbon from two peatland catchments in E. Finland during the spring snowmelt period. *Biogeochemistry*, *103*, 125–142.

Ferrari, G. M., Dowell, M. D., Grossi, S., & Targa, C. (1996). Relationship between the optical properties of chromophoric dissolved organic matter and total concentration of dissolved organic carbon in the southern Baltic Sea region. *Marine Chemistry*, *55*, 299–316.

Gardner, G. B., Chen, R. F., & Berry, A. (2005). High-resolution measurements of chromophoric dissolved organic matter (CDOM) in the Neponset River estuary, Boston Harbor, MA. *Marine Chemistry*, *96*(1–2), 137–154.

Huang, W., & Chen, R. F. (2009). Sources and transformations of chromophoric dissolved organic matter in the Neponset River Watershed. *Journal of Geophysical Research-Biogeosciences*, *114*, 14.

IOCCG (2006). Remote sensing of inherent optical properties: Fundamentals, tests of algorithms, and applications. In Z. P. Lee (Ed.), .

Kirk, J. T. O. (1994). *Light and photosynthesis in aquatic ecosystems.* Cambridge [England]; New York, NY, USA: Cambridge University Press.

Kowalczuk, P., Cooper, W. J., Whitehead, R. F., Durako, M. J., & Sheldon, W. (2003). Characterization of CDOM in an organic-rich river and surrounding coastal ocean in the South Atlantic Bight. *Aquatic Sciences*, *65*, 384–401.

Kutser, T. (2012). The possibility of using the Landsat image archive for monitoring long time trends in coloured dissolved organic matter concentration in lake waters. *Remote Sensing of Environment*, *123*, 334–338.

Kutser, T., Pierson, D. C., Kallio, K. Y., Reinart, A., & Sobek, S. (2005). Mapping lake CDOM by satellite remote sensing. *Remote Sensing of Environment*, *94*, 535–540.

Lee, Z. P., Carder, K. L., & Arnone, R. A. (2002). Deriving inherent optical properties from water color: a multiband quasi-analytical algorithm for optically deep waters. *Applied Optics*, *41*, 5755–5772.

Lee, Z. P., Weidemann, A., Kindle, J., Arnone, R., Carder, K. L., & Davis, C. (2007). Euphotic zone depth: its derivation and implication to ocean-color remote sensing. *Journal of Geophysical Research-Oceans*, *112*.

Mannino, A., Russ, M. E., & Hooker, S. B. (2008). Algorithm development and validation for satellite-derived distributions of DOC and CDOM in the US Middle Atlantic Bight. *Journal of Geophysical Research-Oceans*, *113*, 19.

Nelson, N. B., & Siegel, D. A. (2001). Chromophoric DOM in open ocean. *Biochemistry of marine dissolved organic matter*.

Petsch, S. T., Edwards, K. J., & Eglinton, T. I. (2003). Abundance, distribution and δ13C analysis of microbial phospholipid-derived fatty acids in a black shale weathering profile. *Organic Geochemistry*, *34*, 731–743.

Raymond, P. A., & Bauer, J. E. (2001). Riverine export of aged terrestrial organic matter to the North Atlantic Ocean. *Nature*, *409*, 497–500.

Retamal, L., Bonilla, S., & Vincent, W. F. (2008). Optical gradients and phytoplankton production in the Mackenzie River and the coastal Beaufort Sea. *Polar Biology*, *31*, 363–379.

Retamal, L., Vincent, W. F., Martineau, C., & Osburn, C. L. (2007). Comparison of the optical properties of dissolved organic matter in two river-influenced coastal regions of the Canadian Arctic. *Estuarine, Coastal and Shelf Science*, *72*, 261–272.

Tian, Y. Q., Wang, D. W., Chen, R. F., & Huang, W. (2012). Using modeled runoff to study DOC dynamics in stream and river flow: a case study of an urban watershed southeast of Boston, Massachusetts. *Ecological Engineering*, *42*, 212–222.

Tian, Y. Q., Yu, Q., Ye, C. J., & Blunden, A. (2013). Effects of climate and land-surface process on terrestrial dissolved organic carbon export to major U.S. coastal rivers. *Environmental Engineering*, http://dx.doi.org/10.1016/j.ecoleng.2013.01.028.

Tomlinson, M. C., Stumpf, R. P., Ransibrahmanakul, V., Truby, E. W., Kirkpatrick, G. J., Pederson, B. A., et al. (2004). Evaluation of the use of SeaWiFS imagery for detecting Karenia brevis harmful algal blooms in the eastern Gulf of Mexico. *Remote Sensing of Environment*, *91*, 293–303.

Tranvik, L. J., Downing, J. A., Cotner, J. B., Loiselle, S. A., Striegl, R. G., Ballatore, T. J., et al. (2009). Lakes and reservoirs as regulators of carbon cycling and climate. *Limnology and Oceanography*, *54*, 2298–2314.

Vodacek, A., Blough, N. V., DeGrandpre, M. D., Peltzer, E. T., & Nelson, R. K. (1997). Seasonal variation of CDOM and DOC in the Middle Atlantic Bight: Terrestrial inputs and photooxidation. *Limnology and Oceanography*, *42*, 674–686.

Wynne, T. T., Sturnpf, R. P., Tomlinson, M. C., Ransibrahmanakul, V., & Villareal, T. A. (2005). Detecting Karenia brevis blooms and algal resuspension in the western Gulf of Mexico with satellite ocean color imagery. *Harmful Algae*, *4*, 992–1003.

Yu, Q., Tian, Y. Q., Chen, R. F., Liu, A., Gardner, G. B., & Zhu, W. N. (2010). Functional linear analysis of in situ hyperspectral data for assessing CDOM in rivers. *Photogrammetric Engineering and Remote Sensing*, *76*, 1147–1158.

Zhu, W. N. (2011). Inversion and analysis of chromophoric dissolved organic matter in estuarine and coastal regions using hyperspectral remote sensing. *Ph.D. Dissertation*, Department of Geosciences, University of Massachusetts Amherst.

Zhu, W. N., Tian, Y. Q., Yu, Q., Becker, B., Zheng, T., & Carrick, H. (2012). An Assessment of Remote Sensing Algorithms of Estimating Colored Dissolved Organic Matter in Complex Freshwater Environment, Unpublished Work.

Zhu, W. N., & Yu, Q. (2013). Inversion of chromophoric dissolved organic matter (CDOM) from EO-1 Hyperion imagery for turbid estuarine and coastal waters. *IEEE Transactions on Geoscience and Remote Sensing*, http://dx.doi.org/10.1109/TGRS.2012.2224117.

Zhu, W. N., Yu, Q., Tian, Y. Q., Chen, R. F., & Gardner, G. B. (2011). Estimation of chromophoric dissolved organic matter in the Mississippi and Atchafalaya river plume regions using above-surface hyperspectral remote sensing. *Journal of Geophysical Research-Oceans*, *116*, C02011.